Journal of Inorganic and Organometallic Polymers and Materials (2022) 32:3533–3545
https://doi.org/10.1007/s10904-022-02378-x

Novel Strategy for Hazardous Cement Bypass Dust Removal: Structural, Optical and Nuclear Radiation Shielding Properties of CBD-Bismuth Borate Glass

M. I. A. Abdel Maksoud[1] · O. I. Sallam[2] · Said M. Kassem[3] · Ramy Amer Fahim[3] · A. S. Awed[4]

Received: 6 February 2022 / Accepted: 11 May 2022 / Published online: 9 June 2022
© The Author(s) 2022

Abstract
Herein, this study introduced a novel strategy for hazardous cement bypass dust (CBD) removal via incorporated it into glassy system having the chemical formula $10Li_2O–10Bi_2O_3–(80 - x)B_2O_3–xCBD$, where x = 0, 10, 20 and 30%. The doped glass samples with the CBD were used as a radiation shielding material. The structural, optical and nuclear radiation shielding properties of CBD-lithium bismuth borate (LBB) glass were investigated. The optical energy gap increases from 2.22 eV for LBB + 0% CBD glass sample to 2.66 eV for LBB + 30% CBD glass sample. Also, a comparative study between the experimental data and theoretical interpretation for the attenuation coefficients was addressed via the Phy-X software database. The outcomes unveiled that the shielding parameters such as the linear attenuation coefficient, mass attenuation coefficient, and the effective atomic number were enhanced as CBD content increases. In the same time, the half-value layer, the tenth value layer, and the mean free path are reduced with the enrichment in the CBD content. Furthermore, the exposure build-up factor is inversely related to equivalent atomic numbers. Based on these findings, it was determined that the manufactured bismuth lithium-borate glass system doped cement bypass dust can be used for radiation shielding purposes.

Keywords Cement bypass dust removal · Lithium bismuth borate glass · Optical properties · Radiation shielding properties

1 Introduction

With the perspective increase of population growth in the middle east and north Africa countries and the increase in cement production, it is expected to increase other wastes produced by the cement industry, such as dust dispersed by clinker. Egypt produced almost 30 million tonnes of various types of cement, with 3 million tonnes of cement bypass dust (CBD)/year in dry lines. It has been employed in a variety of cost-effective and helpful applications in various parts of the world. Its contamination has been discovered to be an issue in the vicinity of cement plants. It could have toxic substances in it that are damaging to the environment [1, 2]. The amount of energy released per individual in the developing world could represent its stage of progress. Cement manufacturing is another factor that should be taken into account. However, any industrial activity generates trash that must be managed in order to avoid harmful health and environmental implications [3]. A unique waste material–cement bypass dust (CBD) is a by-product of cement production, which is of less market rate and is primarily relegated to waste where it contributes a risk of groundwater pollution [4].

Radiation has a wide range of applications, but an excessive exposure can have major long-term consequences for human health [5]. As a result, appropriate radiation shielding material has been the most significant topic of research. The conventional materials can shield gamma rays and neutrons. However, it has many disadvantages like toxic, opaque, coast, inflexible, and unsuitable at high

✉ M. I. A. Abdel Maksoud
muhamadmqsod@gmail.com;
muhamad.abdelmaksoud@eaea.org.eg

1 Radiation Physics Department, National Center for Radiation Research and Technology (NCRRT), Egyptian Atomic Energy Authority (EAEA), Cairo, Egypt

2 Radiation Chemistry Department, National Center for Radiation Research and Technology (NCRRT), Egyptian Atomic Energy Authority (EAEA), Cairo, Egypt

3 Radiation Protection and Dosimetry Department, Center for Radiation Research and Technology (NCRRT), Egyptian Atomic Energy Authority (EAEA), Cairo, Egypt

4 Higher Institute for Engineering and Technology, Manzala, Egypt

temperatures. Additionally, another feature is harmful to human health and the surrounding environment. In search of alternative radiation shielding materials, glasses without lead doped by high and low Z elements are being recommended because of its transparency, easy manufacturing, non-toxicity, favorable durability, structural stability, cost-effective, lighter in weight and attenuation coefficients [6]. Numerous studies have been conducted to investigate a variety of radiation shielding glass technologies. The glasses $PbO–Li_2O–B_2O_3$, $BaO–Bi_2O_3–B_2O_3$, $ZnO–Bi_2O_3–B_2O_3$, $Bi_2O_3–Li_2O–Sb_2O_3–B_2O_3$, $B_2O_3–Bi_2O_3–Li_2O$ have been studied [6–10]. The rare-earth ions doped borate glasses, for example, erbium oxide (Er_2O_3), cerium oxide (CeO_2) and tellurium oxide (TeO_2) have various proposes. Their significance is due to chemical stability, corrosion resistance, and low glass transition temperatures, superior mechanical properties, low melting temperatures, high refractive indices and high optical transmittance and had an important role in areas of medical and industrial radiation shielding potential [11, 12]. Different researches have been investigated the incorporation of CBD into glass systems for various applications. Elazaka et al. [13], have incorporated the CBD into $Na_2O–BaCl_2–B_2O_3$ glass system as a nuclear radiation shielding material.

This research aimed to produce a gamma radiation shielding material based on cement bypass dust (CBD) doped with lithium bismuth borate (LBB) glass with composition $10Li_2O–10Bi_2O_3–(80 - x)\ B_2O_3–xCBD$, where (x = 0, 10, 20, and 30%). The LBB + x% CBD (x = 0, 10, 20, and 30) glass samples were characterized via EDX, XRD, FTIR and UV–Vis spectroscopy. Also, the experimental results along with theoretical estimations such as the mass attenuation coefficient (MAC), linear attenuation coefficient (LAC), mean free path (MFP), effective atomic number (Z_{eff}), half value layer (HVL), tenth value layer (TVL) and effective electron density (N_{eff}) were resolved to study the gamma-ray attenuation properties. The exposure build up factor (EBF) and equivalent atomic numbers (Zeq) were also computed. The current examination results would be suitable for special applications on removing hazardous cement bypass dust (CBD) through incorporated it with a glass system to build novel material for gamma radiation shielding.

2 Materials and Methods

2.1 Sample Preparation

In this study, CBD was incorporated with a glass system with composition $10Li_2O–10Bi_2O_3–(80 - x)\ B_2O_3–xCBD$, (LBB + xCBD) where (x = 0, 10, 20 and 30%) (Table 1). The chemical composition of CBD are analyzed by EDX technique that consists of silicon dioxide (SiO_2), aluminium oxide (Al_2O_3), ferric oxide (Fe_2O_3), calcium oxide (CaO), potassium oxide (K_2O), sodium oxide (Na_2O), sulfur trioxide (SO_3), titanium dioxide (TiO_2), manganese oxide (Mn_2O_3) and magnesium oxide (MgO) at 17.14%, 4.96%, 3.37%, 60.33%, 4.82%, 2.46%, 2.64%, 1.17%, 1.09 and 1.02%, respectively. Proper amounts of Li_2O, Bi_2O_3, B_2O_3, and CBD were used in the glass synthesis as previously described in [14, 15]. The thickness of LBB + xCBD where (x = 0, 10, 20 and 30%) samples was found of 2 ± 0.4 mm.

2.2 Characterization Techniques Employed

The traditional Archimedes rule has been utilized to calculate the density of LBB + x% CBD samples at the room temperature as the subsequent equation [16];

$$\rho = \frac{M_a}{(M_{air} - M_{Liquid})}\rho_L \quad (1)$$

where: M_a is the weight of the sample in the air. M_L is the weight of the sample in the distilled water. The molar volume (Vm) of the LBB + x%CBD samples was computed by the following relation,

$$V_m = X_i M_i/\rho \quad (2)$$

where Mi is the molecular weight of the ith component and Xi is the molar fraction of the ith component.

The LBB + x%CBD samples were characterized for their structural properties using X-ray powder diffraction (XRD; Shimadzu XRD-6000) [17–22]. Fourier Transform Infrared (FT-IR) spectroscopy was used to investigate the groups that initiated the LBB + x%CBD samples in range of (4000–400 cm^{-1}). The optical properties of

Table 1 Chemical composition (mole fraction), measured density, molar volume for LBB + x% CBD glasses

Sample code	Mole fraction				Density (ρ) (cm^3/g)	Molar Volume V_m (cm^3)
	Li_2O	Bi_2O_3	B_2O_3	CBD		
LBB + 0%CBD	10	10	80	0	2.965	35.528
LBB + 10%CBD	10	10	70	10	2.988	35.124
LBB + 20%CBD	10	10	60	20	3.046	34.298
LBB + 30%CBD	10	10	50	30	3.169	32.838

LBB + x%CBD samples were illustrated in the wavelength range 300–1100 nm via UV–Vis spectrophotometer [15, 23].

2.3 Shielding Parameters Simulation

A fine beam transmission scheme has been applied to measure the gamma ray effectiveness parameters for LBB + x% CBD samples as represented in Fig. 1. The ^{137}Cs (1 μCi) and ^{60}Co (1 μCi) gamma ray point sources were utilized in this study as well as a NaI (Tl) scintillation detector with a 3″ × 3″ powerful crystal location. The gamma-ray detector held attached to Canberra Genie-2000 software for the data interpretation. Furthermore, the Phy-X /PSD software was accepted in order to calculate the gamma-ray shielding characteristics of LBB + x%CBD samples at different energies from 0.001 to 15 MeV [24, 25].

3 Results and Discussion

3.1 Structural Analyses

Figure 2 shows the XRD patterns of LBB + x% CBD glass samples. The figure reveals that the samples displayed a broad amorphous hump at 2θ ~ 28° and there is non-attendance of sharp peaks [26, 27]. This gives confirmation of the glassy state of the prepared samples. Besides, there a small peak appeared in the range ($2\theta = 10°–20°$) for LBB + 30% CBD sample, which may be related to the presence of second phase (ceramic/glass) due to increasing the CBD doping ratio [28–30].

Figure 3 exhibited the FTIR spectra of LBB + x% CBD glass samples. The figure tells a clear explanation about the chemical structure of the prepared cement-glass samples, and the changes that occurred upon increasing CBD concentration in the wavenumber range from 400 to 4000 cm^{-1}. In case of base glass (LBB + 0% CBD); the spectra admit four main absorption peaks at 520, 690, 955 and 1300 cm^{-1}. In general, boron atoms are found inside the glass network as tetraborate units (BO_4) and boroxol rings. The tetraborate units can be broken to give NBO (non-bridging oxygen) upon addition any cation which results from other additives to the structure as former or modifiers [31]. Bi^{3+} can be

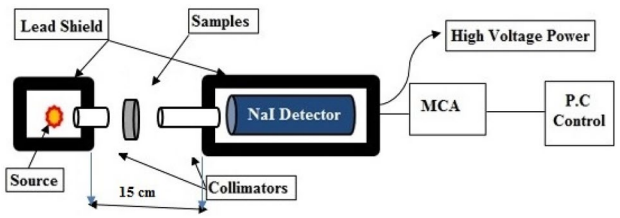

Fig. 1 The experimental setup for LBB + x%CBD glass

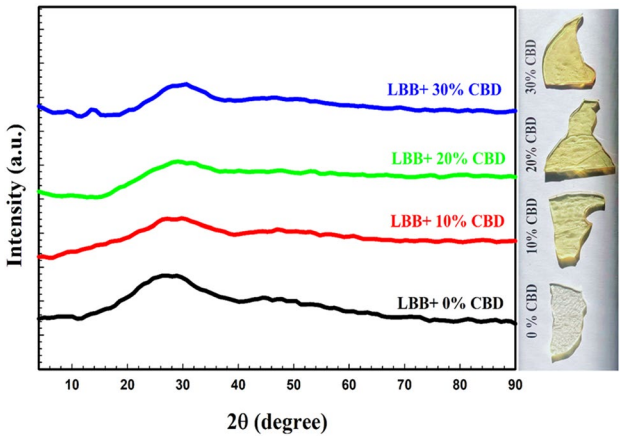

Fig. 2 XRD patterns of LBB + x% CBD glass samples

settled inside the glass network by ionic bond between Bi^{3+} ion and oxygen atoms bonded to borate network as a result of the previous rupture occurred from borate units so bismuth borate glasses can show two bands; one at 850 cm^{-1} for BiO_3 units and another one at 540 cm^{-1} for BiO_6 (octahedron) [32, 33].

Figure 3 gives four broad regions due to the amorphous nature and the well homogenous distribution of the component inside the glass matrix. The first three regions can be decovoluted to illustrate the overlap peaks under these regions as given by Fig. 4a and b. All observed peaks are shown at Table 2.

Upon introducing and increment of CBD concentration by (x = 10, 20 and 30%) in bismuth-borate glass; some observations are detected as follow:

(a) relative area for bands in the ranges from 1245 to 1450 cm^{-1} decreased by increased cement dust concentration due to the formation of BO_3 from BO_4

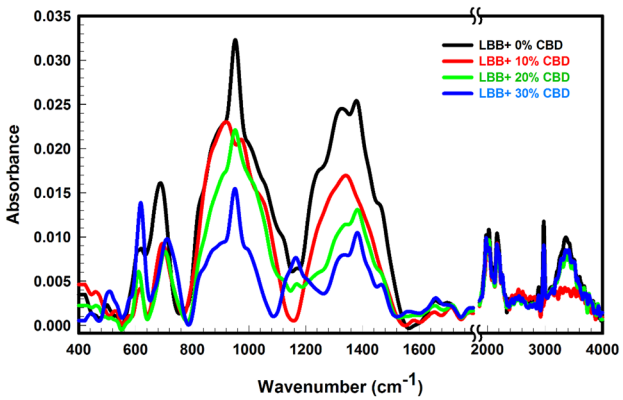

Fig. 3 FTIR spectra of LBB + x% CBD glass samples

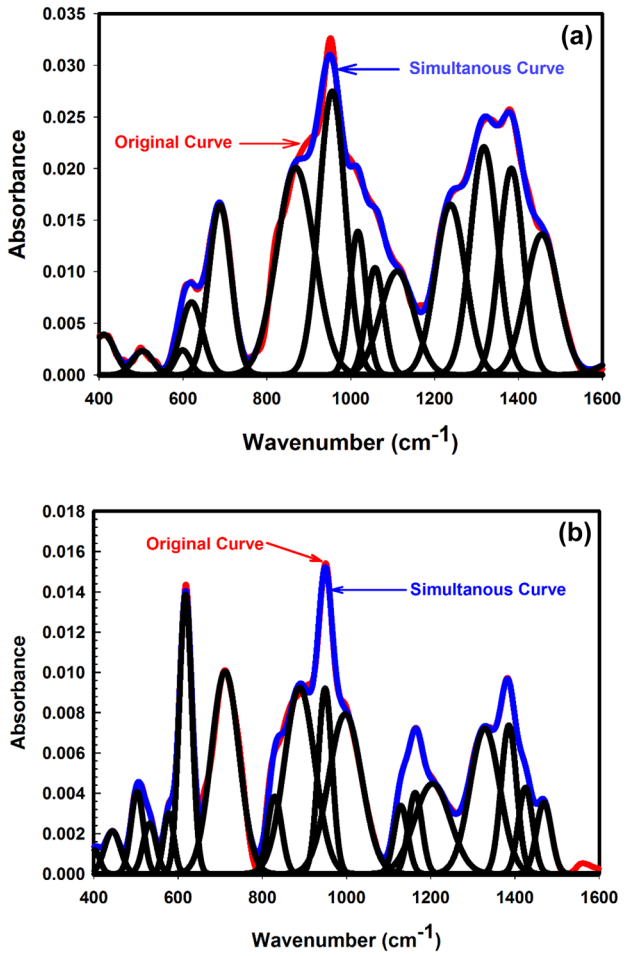

Fig. 4 Deconvoluted FTIR spectra of LBB + x% CBD glass with **a** 0% CBD, **b** 30% CBD

(b) Peak at 520 cm^{-1} give higher intensity for 30% cement dust
(c) Lowering in borate group intensity due to the breaking in borate bonds and formation of NBO and at the same time decreasing of OH and H_2O groups inside the network as CaO introduced.
(d) Position of some bonds show shift to higher values of wavenumber

The first three regions can be decovoluted to illustrate the overlap peaks under these regions as given by Figs. 3 and 4 with their relative area (A) and band center (C) in wavenumber range from 400 to 1800 cm^{-1} as shown in Table 3. These parameters help in calculating (N4) values for each sample where:

$$N_4 = BO_4/(BO_3 + BO_4)$$

N_4 value can confirm how the transformation from BO_3 into BO_4 units is; only one oxygen atom for each transformation is needed to finish this process. Upon the addition of cement bypass dust, N_4 values increase due to the decrease of the area and shifted of most of the peaks to higher wavenumbers due to the formation of (SiO_4 and CaO_4) units and the tendency of conversion from BO_3 to BO_4 by creating calcium silicate covalent bonds inside the borate glassy network which raise the yield of non-bridging oxygen [31] by filling the positions between boron-oxygen linkage with Ca^{2+} and Si^{4+} that meaning the glass network become more lose. N_4 results are confirmed by density values as by adding more cement dust to bismuth borate glass, the density increase gradually, so the compactness of the glass network increases. This behavior suggested that our samples can be used for many purposes, including radiation shielding.

3.2 Optical Behavior

Figure 5 presents the transmittance (T) of LBB + x% CBD glass samples. In Fig. 5, the transmittance edges in the visible region were showed a shift to a higher wavelength (λ) as the CBD' concentration was increased [42–44]. Besides, it is clear that in IR region, the transmittance was increased with the increase in CBD' concentration except for the decrease that occurred at x = 20%. This behavior can be attributable to the defects variation and the localized electronic states in the glass lattice between the highest occupied molecular orbital (HOMO) and the lowest unoccupied molecular orbital (LUMO) band edges [45]. These parameters lead to appearing the changing in the energy transitions available as a result of CBD' addition [23, 46]. This behavior was previously seen in [14]. Radiation-shielded windows are commonly employed to give total protection while providing visibility into the protected room's operations. As a result, it should be transparent rather than opaque.

Also, Fig. 6 illustrates the extinction coefficient k of LBB + x% CBD glass samples [47]. The extinction coefficient k is represented the light lost ascribing to scattering and absorption by unit volume. Therefore, great values of k in the lower wavelength area confirm that these materials are opaque in this area [48]. The addition of CBD to LBB glass shifted the absorption edge for the higher wavelength in the visible area [14, 49, 50].

The indirect bandgap can be obtained via plotting $(\alpha h\nu)^{1/2}$ vs ($h\nu$) for LBB + x% CBD glass samples (Fig. 7). The optical energy gap increases from 2.22 eV for LBB + 0% CBD glass sample to 2.66 eV for LBB + 30% CBD glass sample due to the addition of CBD to LBB glass [51]. The increase in Eg values can be ascribed to a change in LBB glass structure and the generation of defects in charge distribution as a result of the addition of CBD concentration through enhancing the energy state of the oxygen ions and the degree of localization. It should be highlighted that all

Table 2 FTIR peaks and their assignment for LBB + x% CBD glass samples

Peak (cm^{-1})	Assignment
Area (I) 400–800 cm^{-1} (Cation region)	
430	Vib. of Fe^{3+} cations[34]
450	Vib. of Li^{3+} cations [31]
520	Vib. of Ca^{2+} cations [34, 35]
540	Bi–O–Bi and Bi–O in BiO_6 octahedral group [32, 36]
590	Bend. Vib. O–Si–O and Si–O–Si in SiO_4 unit (tetrahedral) [35, 37]
620	Vib. of BO_4 group
690	Bend. Vib. of B–O–B of BO_3 groups
Area (II) 800–1155 cm^{-1} (Tetragonal Units) (BO_4 units)	
820	Bend. Vib. of Si–O–Si of (SiO_4) groups[38]
865	For BiO_3 groups[32]
950	Str. Vib. of B–O in diborate BO_4 groups[32]
1050	Str. Vib. of B–O in triborate BO_4 groups and may be for Si–O–B linkage[39]
1100	Str. Vib. of B–O in tetraborate BO_4 groups[31]
1150	Str. Vib. of B–O in pentaborate BO_4 groups [31]
1155	Str. Vib. of CaO_6 units
Area (III) 1155–1640 cm^{-1} (Triagular Units) (BO_3 units)	
1245	Vib. of BO3 groups (meta, ortho, pyro)
1345	Vib. of BO3 groups (meta, ortho, pyro)
1450	Antisym. Str. Vib. of 3 NBO of B–O–B of BO_3 units[31]
1650	Str. B–O of BO3
Area (IV) Above1640 cm^{-1} (near IR region)	
1980	(SiOH) silanol units[40]
2160, 2975 and 3370	Str. vib. of OH and hydroxyl units beside the bending vib. from H–O–H bonds[41]

Table 3 De-convolution parameter of the infrared spectra of studied glasses, (C) is the component band center and (A) is the relative area (%) of the samples bands (0, 10, 20, 30% CBD)

Sample	x% CBD							
	0%		10%		20%		30%	
Deconvelotion parameters	C	A	C	A	C	A	C	A
Peak 1	411	0.258	401	0.454	401	0.185	401	0.061
Peak 2	503	0.141	431	0.145	436	0.099	444	0.100
Peak 3	599	0.109	469	0.148	470	0.085	502	0.150
Peak 4	–	–	525	0.016	512	0.034	532	0.096
Peak 5	–	–	550	0.063	555	0.060	577	0.092
Peak 6	620	0.459	614	0.131	611	0.209	617	0.518
Peak 7	688	1.092	697	0.627	704	0.824	711	0.825
Peak 8	–	–	850	1.172	846	0.698	829	0.161
Peak 9	868	2.272	914	1.539	902	0.578	888	0.836
Peak 10	955	2.160	978	1.324	960	1.058	949	0.384
Peak 11	1017	0.679	1050	1.024	1038	0.747	996	0.779
Peak 12	1058	0.539	1098	0.119	1106	0.383	1129	0.137
Peak 13	1110	1.000	1211	0.156	1176	0.310	1163	0.164
Peak 14	–	–	1248	0.184	1239	0.395	1204	0.476
Peak 15	1237	1.489	1287	0.612	1297	0.618	1328	0.638
Peak 16	1317	1.795	1343	1.683	1340	0.598	1385	0.341
Peak 17	1383	1.438	1429	0.198	1389	0.954	1424	0.181
Peak 18	1455	1.331	1475	0.103	1455	0.585	1468	0.157
N_4 value	0.459		0.469		0.475		0.499	

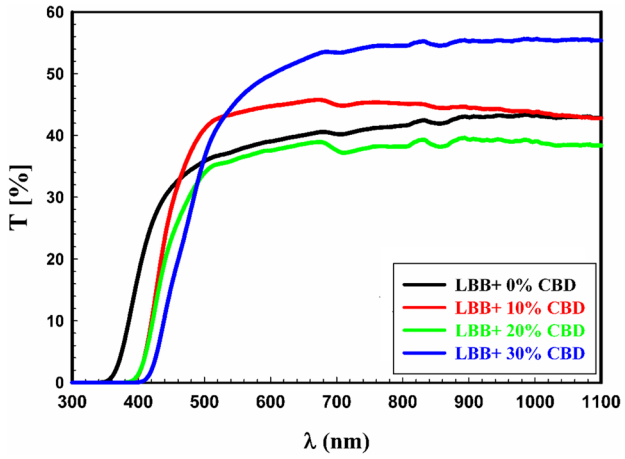

Fig. 5 the transmittance (T) spectra of LBB + x% CBD glass samples

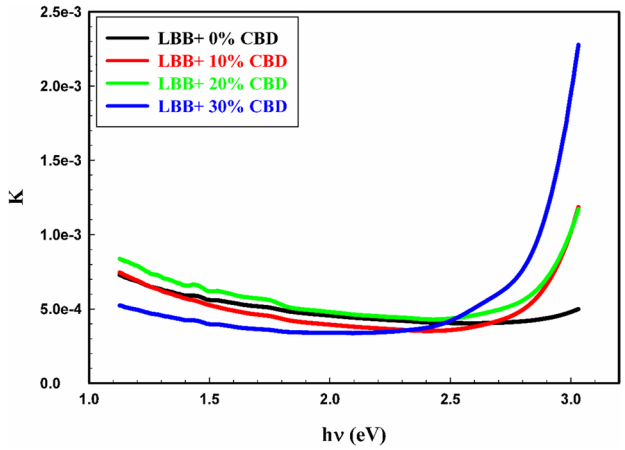

Fig. 6 The extension coefficient (k) vs. hν of LBB + x% CBD glass samples

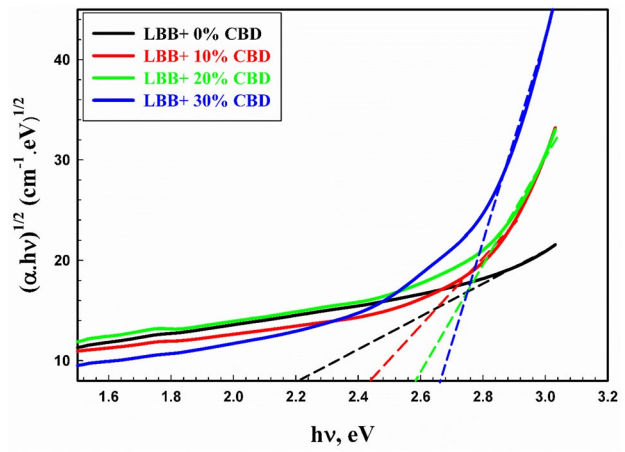

Fig. 7 relation between $(\alpha h\nu)^{1/2}$ vs $(h\nu)$ for LBB + x% CBD glass samples

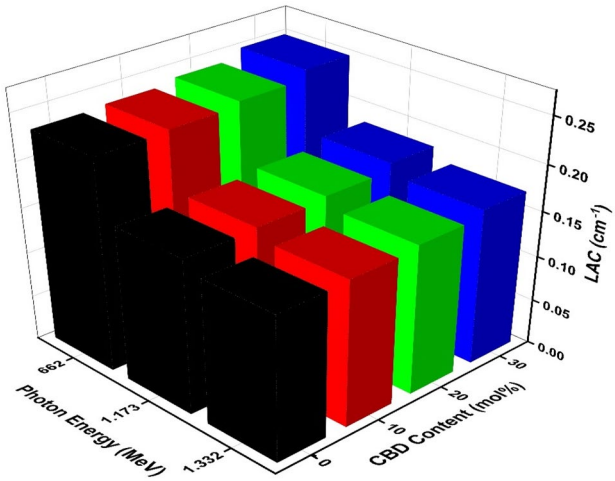

Fig. 8 Linear attenuation coefficients for LBB + x% CBD glass samples

data show an increase in NBO in the glass matrix, which causes an increase in O^{2-} ions [52].

3.3 Radiation Shielding Properties

By analyzing the spectrum of emitted gamma rays across an absorber of a specific thickness, the gamma-ray attenuation capabilities were investigated for the glass barriers under study. Lambert-law Beer's was utilized to get linear attenuation coefficient (LAC) parameter for the investigated glass samples using gamma rays narrow beam system of ^{60}Co and ^{137}Cs that can be computed by the following equation.

$$I_{(d)} = I_o e^{LAC*d} \quad (3)$$

where (d) is the thickness of sample, I_0 is the intensity of incident gamma rays without absorber, and I_d is the intensity of incident gamma rays with absorber thickness (d).

The gamma-ray effectiveness relations did apply to assess the attenuation parameters LAC, MAC, HVL, TVL, MFP, Neff and Zeff of the LBB + x% CBD samples according to equations as presented in [14, 16, 24].

Along with all specified photon energies, Fig. 8 displays the LAC values in a relationship to CBD content. That shows LAC increases as CBD content increase due to adding more elements have gamma-ray absorption effect, which increases the molecular weight of the sample as well as density increase (such as, Fe_2O_3, TiO_2, Al_2O_3, SiO_2, Mn_2O_3, MgO and CaO) [9, 13, 14].

By comparing the gamma-ray mass attenuation coefficient of the prepared samples with ordinary concrete (OC) and barite concrete (BC) at 662 keV, it was found of 0.07889, 0.084 and 0.0857 cm^2/g, respectively. In addition, it is observed that the sample 30% CBD has the lowest

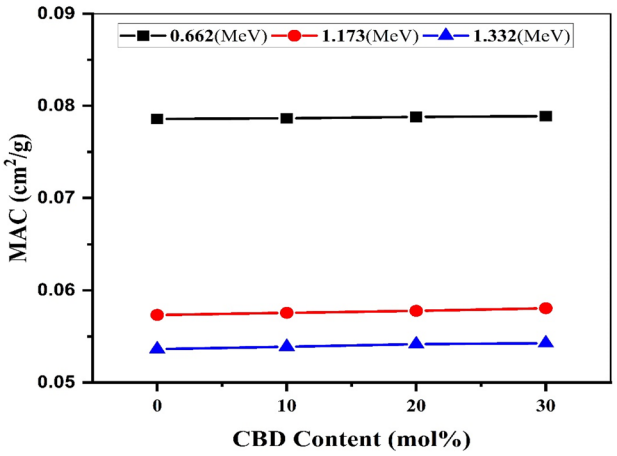

Fig. 9 Mass attenuation coefficients for LBB + x% CBD glass samples

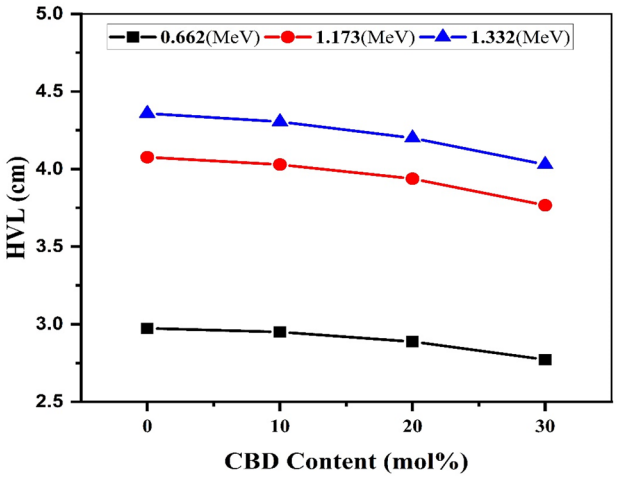

Fig. 10 HVL values for LBB + x% CBD glass samples

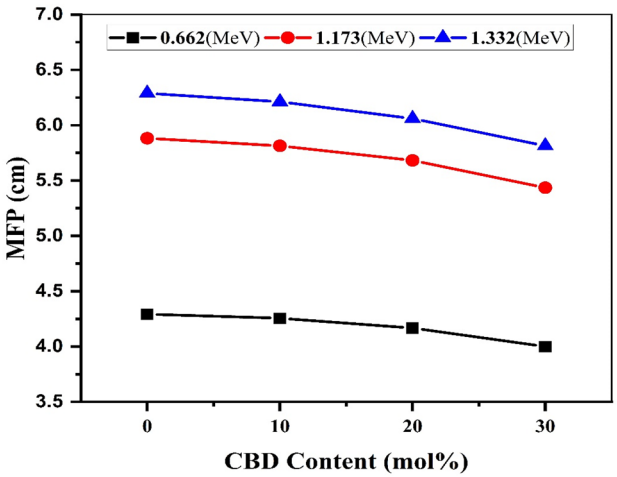

Fig. 11 MFP values for LBB + x% CBD glass samples

Table 4 Theoretical (MAC) Phy-X and experimental mass attenuation coefficient (MAC)exp (cm^2/g) for LBB + x% CBD glass samples

CBD mol%	Phy-X	EXP	Diff
662 MeV			
0	0.0785	0.07858	0.105732
10	0.07867	0.07865	0.027965
20	0.07884	0.07879	0.060883
30	0.07901	0.07889	0.153145
1.173 MeV			
0	0.0577	0.05734	0.630849
10	0.05781	0.05756	0.425532
20	0.05792	0.05778	0.239986
30	0.05803	0.05806	0.055144
1.332 MeV			
0	0.0539	0.05363	0.508349
10	0.054	0.05388	0.218519
20	0.05411	0.05417	0.109037
30	0.05421	0.05427	0.11437

Diff = |(Phy-X − EXP.)/Phy-X | × 100

values of the mean free path compared to the mean free path for ordinary concrete, hematite-serpentine concrete and ilmenite-limonite concrete at the 662 keV energy are 5.5957, 5.2219 and 4.6038 cm respectively. Therefore, the substitution of the ordinary gamma-ray shielding materials by low weight, reusing hazardous by-products, transparent shield, relatively efficient attenuator and low coast manufactured material was much gained [53–55].

Figure 9 illustrates the MAC values as a relationship of CBD content for all particular photon energies. Table 4 shows a contrast of computed MAC values LBB + x% CBD glass samples and gamma ray energy. It can be observed that the experimental data obtained and the numerical simulations are in reasonable conformity.

The HVL, MFP, and TVL are depicted in Figs. 10, 11, and 12. The HVL, MFP, and TVL values decreases as the CBD content in the LBB glass increasing, as shown in those graphs. As well as the gamma rays energies increases these values increase [6, 54]. Therefore, it may be confirmed that addition of CBD to the LBB glass increases the system's shielding properties.

Figures 13 and 14 illustrated the Z_{eff} and N_{eff} values for LBB + x% CBD glass samples at given gamma rays energies (662, 1.173 and 1.332 MeV) were increased with increasing CBD concentration (Table 5). Conversely, when photon energy increase, both Z_{eff} and N_{eff} values reduced for LBB + x% CBD samples. In addition, Table 5 shows that the total atomic cross section (σ_t) and the total electronic cross

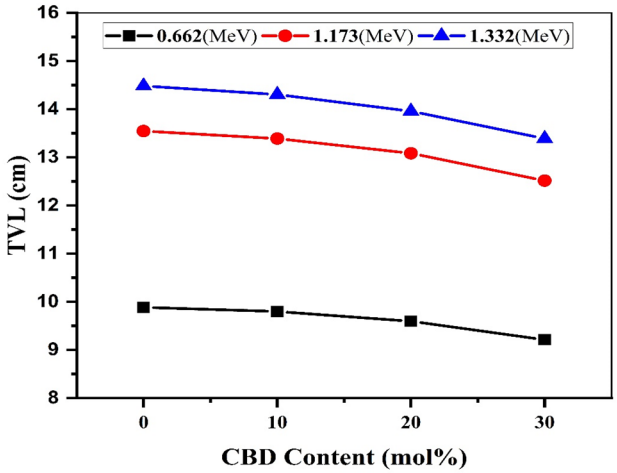

Fig. 12 TVL values for LBB + x% CBD glass samples

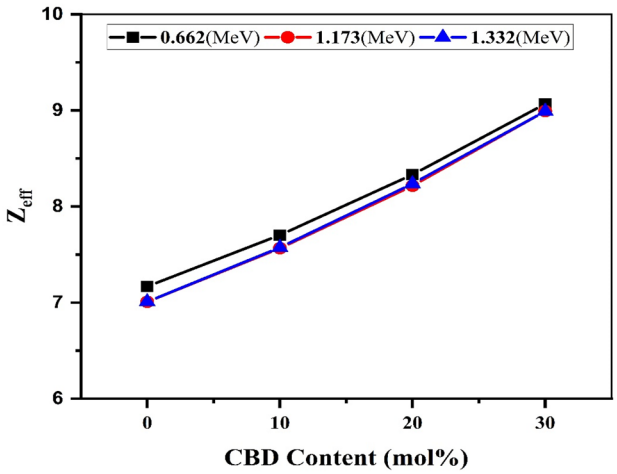

Fig. 13 Variation of effective atomic number (Z_{eff}) with for LBB + x% CBD glass samples

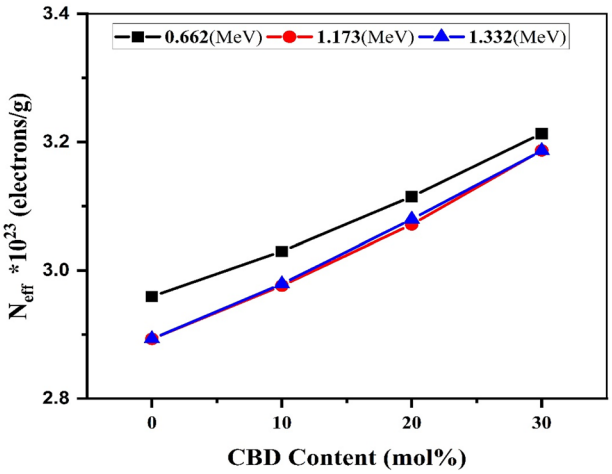

Fig. 14 Variation of effective electron number (N_{eff}) for LBB + x% CBD glass samples

section (σ_e) values for LBB + x%CBD glass samples. All of these variables exhibit nearly identical response to that of MAC as energy dependence and CBD content.

Figure 15 shows the EBF against gamma rays energy charts for LBB + x%CBD samples at different penetration depths of 1, 5, 10, 15, 20, 25, 30, 35 and 40 mfp. The steep peaks in the graphs are caused by bismuth absorption edges**.** The EBF grows with a depth and reaches extreme value at 40 mfp. Several scattering reactions result in the creation of secondary gamma rays at deeper penetration depths [54, 56, 57].

The fluctuation of EBF with penetration depth (mfp) for the glass samples has been estimated and can be seen in Fig. 16 for gamma rays energies of 0.015, 0.15, 1.5, 3, 8, 15 MeV. The EBF values are mfp independent at the low energy range (0.015, 0.15 MeV) and lowest values. The gamma rays photons are fully cancelled out due of the photoelectric effect in this energy band. In the intermediate energy area, EBF has a linear relationship with mfp. The EBF improved within repeated Compton scattering at higher gamma-ray energies [6]. Furthermore, in the low and intermediate energy zones, an inverse relation between EBF and the equivalent atomic number (Zeq), whereas in the higher energy region, it is roughly related to Z_{eq} (Fig. 17). This occurs due to the pair production phenomenon is the most important interacting activity in the higher energy area.

At middle photon energy region the EBF is lowest for LBB + 30% CBD (30 mol% CBD) and in dissimilarity, the EBF is lowest for LBB + 0% CBD (0 mol% CBD) in higher photon energy area (Fig. 16). Hence, the choice of appropriate radiation shielding material be influenced by the incident radiation energy in a specific application [9, 58].

4 Conclusions

This study displayed a novel strategy for removing hazardous cement bypass dust (CBD) by incorporating it into a glassy system with the chemical formula $10Li_2O–10Bi_2O_3–(80 - x)B_2O_3–xCBD$, where x = 0, 10, 20, and 30%. Further, the LBB + x% CBD glass samples possess an additional function as a candidate material for radiation shielding applications. Also, the structural, optical, and attenuation properties of the LBB + x% CBD glass samples have studied. The optical energy gap increases from 2.22 eV for LBB + 0% CBD glass sample to 2.66 eV for LBB + 30% CBD glass sample. The increase in E_g values can be ascribed to a change in LBB glass structure and the generation of defects in charge distribution due to the addition of CBD concentration. The MAC values were

Table 5 The total atomic cross section (σ_t), the total electronic cross section (σ_e), the effective atomic number (Z_{eff}), and the electron density (N_{eff}) for LBB + x% CBD glass samples

CBD mol%	$\sigma_t \times 10^{-24}$ (cm^2/g)	$\sigma_e \times 10^{-25}$ (cm^2/g)	Z_{eff}	$N_{eff} \times 10^{23}$ (e^-/g)
662 MeV				
0	1.9035	2.6555	7.17	2.9592
10	1.9995	2.5959	7.70	3.0297
20	2.1076	2.5296	8.33	3.1148
30	2.2263	2.4553	9.07	3.2131
1.173 MeV				
0	1.3888	1.9818	7.01	2.8931
10	1.4634	1.9343	7.57	2.9760
20	1.5456	1.8813	8.22	3.0713
30	1.6386	1.8220	8.99	3.1867
1.332 MeV				
0	1.2989	1.8535	7.01	2.8932
10	1.3698	1.8088	7.57	2.9788
20	1.4490	1.7591	8.24	3.0794
30	1.5316	1.7033	8.99	3.1863

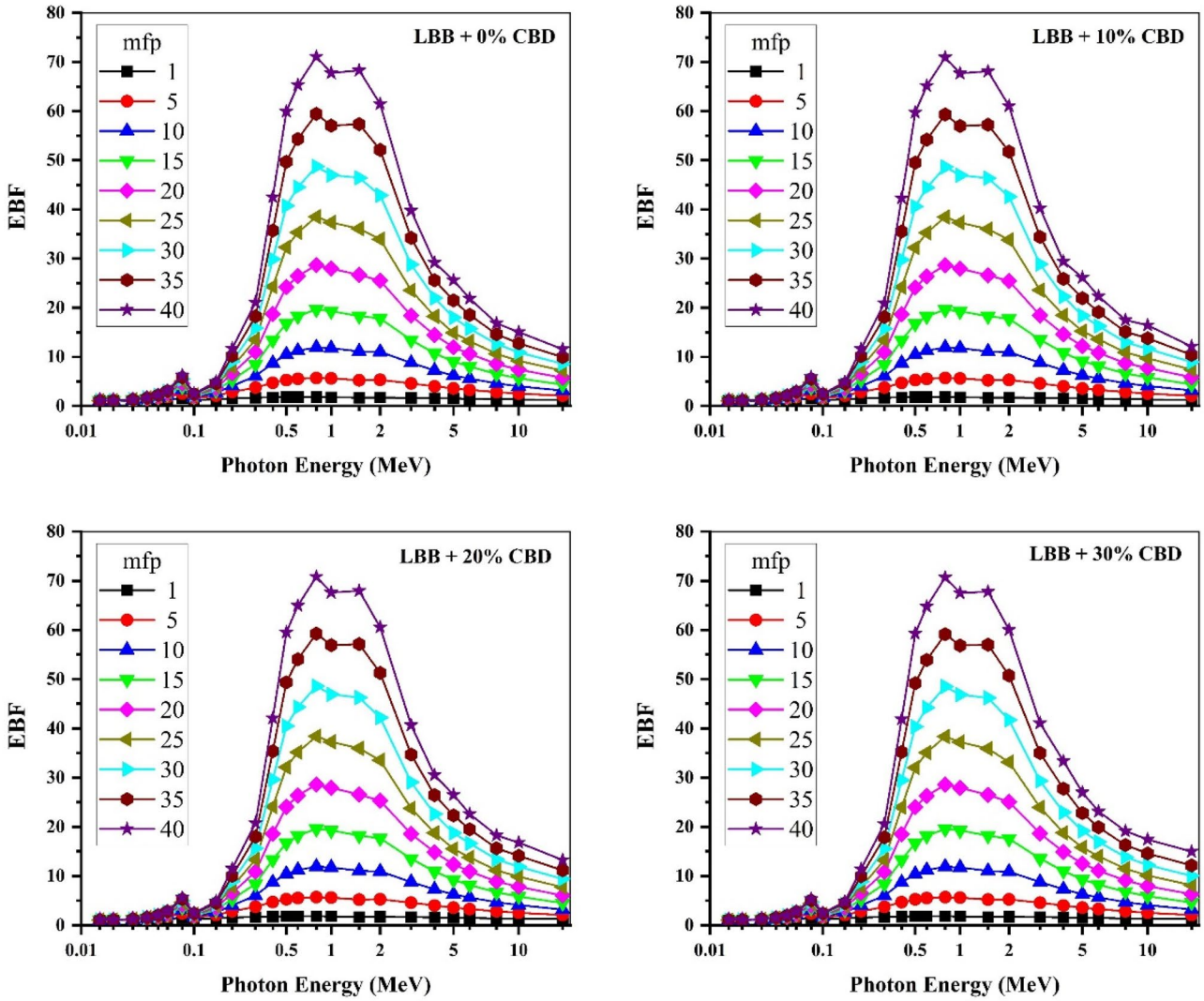

Fig. 15 The EBF versus photon energy for LBB + x% CBD glass samples at various penetration depths

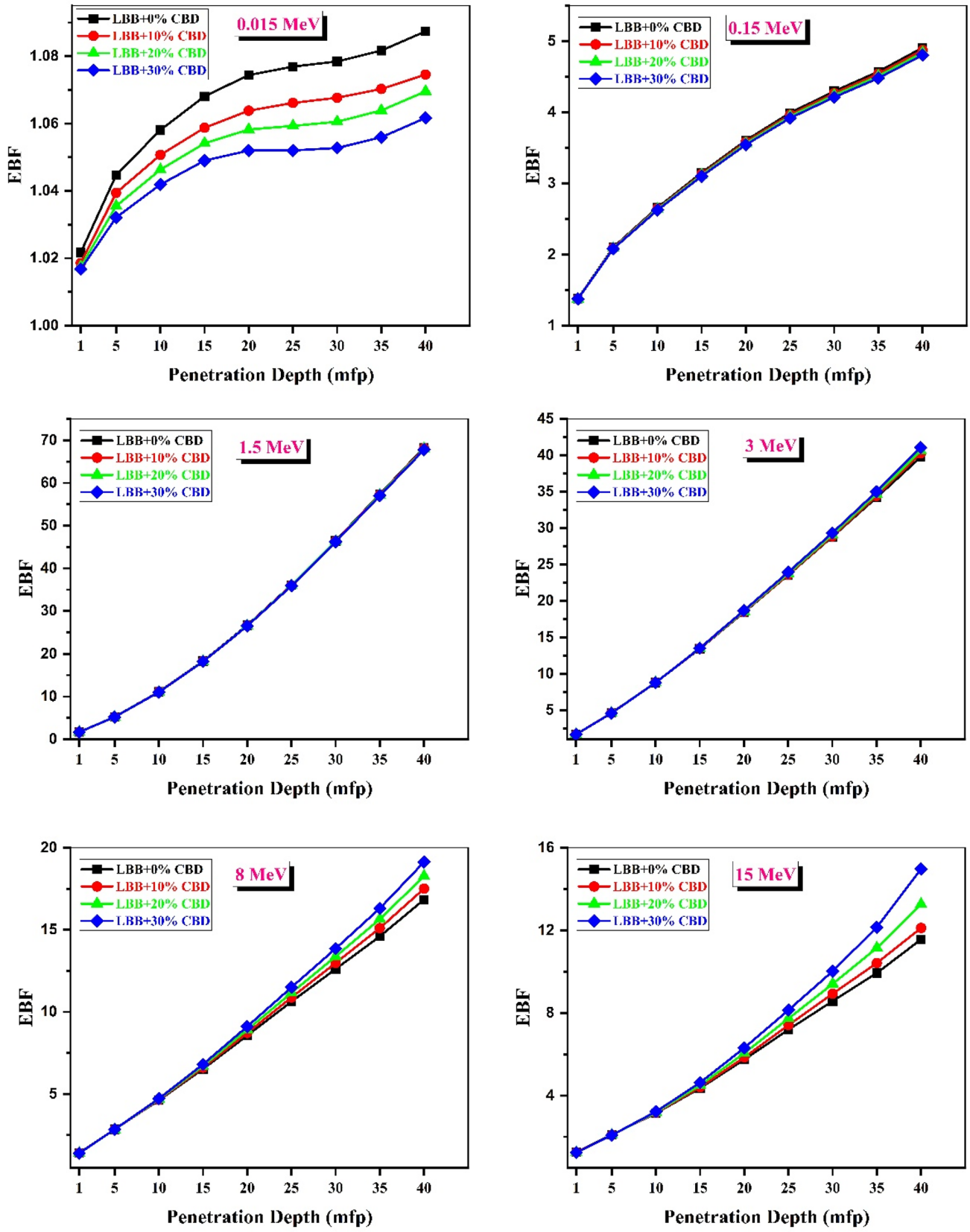

Fig. 16 The EBF versus the penetration depth for LBB + x% CBD glass samples at various photon energies

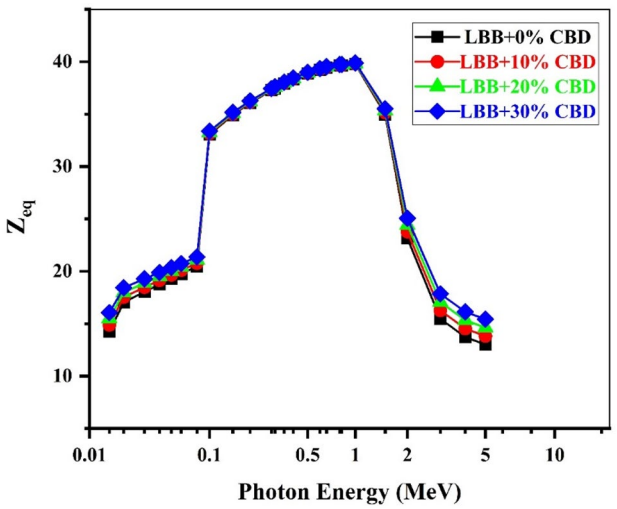

Fig. 17 Variation of Z_{eq} concerning EBF for LBB + x% CBD glass samples

calculated using the Phy-X database code, and experiments. The LAC and MAC values are enhanced as the CBD substituent ratio increases. The MFP and HVL values declined as the CBD substituent ratio increased in the same context. By comparing the gamma-ray mass attenuation coefficient of the prepared samples with ordinary concrete (OC) and barite concrete (BC), it was found to be promising. Furthermore, a good matching between the experimental results and theoretical calculations was observed, indicating the Phy-X code's efficiency. Besides, it is noticed that the best sample for gamma-ray shielding is LBB + 30% CBD. Choosing a suitable shield material with the best thickness for radiation shielding could be accomplished using data from the tenth value layer, considering the exposure build-up factor, the energy of incident radiation, and the particular applications. Overall, the structural, optical, and attenuation properties of the LBB + x%CBD glass samples make them candidate materials for radiation shielding applications.

Funding Open access funding provided by The Science, Technology & Innovation Funding Authority (STDF) in cooperation with The Egyptian Knowledge Bank (EKB). None.

Data Availability Not applicable.

Declarations

Conflict of interest The authors declare that they have no conflict of interest.

Ethical Approval Not required.

Informed Consent Not applicable.

Consent to Publish Not applicable.

Open Access This article is licensed under a Creative Commons Attribution 4.0 International License, which permits use, sharing, adaptation, distribution and reproduction in any medium or format, as long as you give appropriate credit to the original author(s) and the source, provide a link to the Creative Commons licence, and indicate if changes were made. The images or other third party material in this article are included in the article's Creative Commons licence, unless indicated otherwise in a credit line to the material. If material is not included in the article's Creative Commons licence and your intended use is not permitted by statutory regulation or exceeds the permitted use, you will need to obtain permission directly from the copyright holder. To view a copy of this licence, visit http://creativecommons.org/licenses/by/4.0/.

References

1. W.S. Adaska, D.H. Taubert, Beneficial uses of cement kiln dust, in: *2008 IEEE Cement Industry Technical Conference Record*, IEEE, 2008, pp. 210–228.
2. H. Hassan, M. Morsy, G. El-Dawwy, K.H. Mohammed, Environmental monitoring and risk assessment of the soil pollution around two cement factories in EL-Minia Governorate, Egypt. J. Modern Res. **2**(2), 105–114 (2020)
3. E. Terpáková, N. Števulová, Trends in the use of cement bypass dusts for their application in construction, Key Engineering Materials, Trans Tech Publ, 2020, pp. 39–45.
4. R. Siddique, *Waste Materials and By-products in Concrete* (Springer Science & Business Media, New York, 2007)
5. M.A.S. Sherer, P.J. Visconti, E.R. Ritenour, K. Haynes, *Radiation Protection in Medical Radiography-E-Book* (Elsevier Health Sciences, Amsterdam, 2021)
6. P. Kaur, K.J. Singh, S. Thakur, M. Kurudirek, M.M. Rafiei, Structural investigations and nuclear radiation shielding ability of bismuth lithium antimony borate glasses. J. Phys. Chem. Solids **150**, 109812 (2021)
7. A. Kumar, Gamma ray shielding properties of PbO-Li_2O-B_2O_3 glasses. Radiat. Phys. Chem. **136**, 50–53 (2017)
8. M.I. Sayyed, S.A.M. Issa, H.O. Tekin, Y.B. Saddeek, Comparative study of gamma-ray shielding and elastic properties of BaO–Bi_2O_3–B_2O_3 and ZnO–Bi_2O_3–B_2O_3 glass systems. Mater. Chem. Phys. **217**, 11–22 (2018)
9. A.M. Vadavathi, S.K. Chinthakayala, V.S. Kollipara, G. Ramadurai, P. Gadige, Physical properties and gamma radiation shielding capability of highly dense binary bismuth borate glasses. Ceram. Int. **47**(7), 9791–9805 (2021)
10. G. Lakshminarayana, A. Kumar, H.O. Tekin, S.A.M. Issa, M.S. Al-Buriahi, M.G. Dong, D.-E. Lee, J. Yoon, T. Park, Probing of nuclear radiation attenuation and mechanical features for lithium bismuth borate glasses with improving Bi_2O_3 content for B_2O_3 + Li_2O amounts. Results Phys. **25**, 104246 (2021)
11. B. Aktas, A. Acikgoz, D. Yilmaz, S. Yalcin, K. Dogru, N. Yorulmaz, The role of TeO_2 insertion on the radiation shielding, structural and physical properties of borosilicate glasses. J. Nucl. Mater. **563**, 153619 (2022)
12. A. Acikgoz, G. Demircan, D. Yılmaz, B. Aktas, S. Yalcin, N. Yorulmaz, Structural, mechanical, radiation shielding properties and albedo parameters of alumina borate glasses: role of CeO_2 and Er_2O_3. Mater. Sci. Eng., B **276**, 115519 (2022)
13. A.I. Elazaka, H.M.H. Zakaly, S.A.M. Issa, M. Rashad, H.O. Tekin, H.A. Saudi, V.H. Gillette, T.T. Erguzel, A.G. Mostafa, New approach to removal of hazardous Bypass Cement Dust (BCD) from the environment: 20Na_2O–20$BaCl_2$–(60 − x)

B_2O_3–(x)BCD glass system and optical, mechanical, structural and nuclear radiation shielding competences. J. Hazard. Mater. **403**, 123738 (2021)
14. M.I.A. Abdel Maksoud, E.M. Abou Hussein, S.M. Kassem, R.A. Fahim, A.S. Awed, Effect of CeO_2 addition on structural, optical, and radiation shielding properties of B2O3–Na2O–SrO glass system. J. Mater. Sci. **32**(14), 18931–18950 (2021)
15. E.M. Abou Hussein, M.I.A. Abdel Maksoud, R.A. Fahim, A.S. Awed, Unveiling the gamma irradiation effects on linear and nonlinear optical properties of CeO_2–Na_2O–SrO–B_2O_3 glass. Optic. Mater. **114**, 111007 (2021)
16. S.M. Kassem, G. Ahmed, A. Rashad, S. Salem, S. Ebraheem, A. Mostafa, An investigation of the nuclear shielding effectiveness of some transparent glasses manufactured from natural quartz doped lead cations. Nucl. Eng. Technol. **53**(6), 2025–2037 (2021)
17. E.K. Abdel-Khalek, D.A. Rayan, A.A. Askar, M.I.A.A. Maksoud, H.H. El-Bahnasawy, Synthesis and characterization of $SrFeO_3$-δ nanoparticles as antimicrobial agent. J. Sol-Gel. Sci. Technol. **97**(1), 27–38 (2021)
18. A.S. Awed, M.I.A.A. Maksoud, M.M. Atta, R.A. Fahim, Nonlinear optical properties of irradiated 1,2-dihydroxyanthraquinone thin films: merged experimental and TD-DFT insights. J. Mater. Sci. **30**(8), 7858–7865 (2019)
19. M.A. Maksoud, M.M. Ghobashy, G.S. El-Sayyad, A.M. El-Khawaga, M.A. Elsayed, A. Ashour, Gamma irradiation-assisted synthesis of PANi/Ag/MoS_2/$LiCo_{0.5}Fe_2O_4$ nanocomposite: efficiency evaluation of photocatalytic bisphenol A degradation and microbial decontamination from wastewater. Optic. Mater. **119**, 111396 (2021)
20. M. Abdel Maksoud, A. El-Ghandour, G.S. El-Sayyad, R.A. Fahim, A.H. El-Hanbaly, M. Bekhit, E. Abdel-Khalek, H. El-Bahnasawy, M. Abd Elkodous, A. Ashour, Unveiling the effect of Zn^{2+} substitution in enrichment of structural, magnetic, and dielectric properties of cobalt ferrite. J. Inorg. Organomet. Polym. Mater. **30**(9), 3709–3721 (2020)
21. M. Maksoud, G.S. El-Sayyad, M. Abd El-Kodous, A. Awed, Controllable synthesis of $Co_{1-x}M_xFe_2O_4$ nanoparticles (M= Zn, Cu, and Mn; x = 0.0 and 0.5) by cost-effective sol-gel approach: analysis of structure, elastic, thermal, and magnetic properties. J. Mater. Sci. **31**(12), 9726–9741 (2020)
22. M.A. Maksoud, G.S. El-Sayyad, H.S. El-Bastawisy, R.M. Fathy, Antibacterial and antibiofilm activities of silver-decorated zinc ferrite nanoparticles synthesized by a gamma irradiation-coupled sol–gel method against some pathogenic bacteria from medical operating room surfaces. RSC Adv. **11**(45), 28361–28374 (2021)
23. B. Alshahrani, H.I. ElSaeedy, S. Fares, A.H. Korna, H.A. Yakout, A.H. Ashour, M.I.A. Abdel Maksoud, R.A. Fahim, A.S. Awed, Revealing the effect of gamma irradiation on structural, ferromagnetic resonance, optical, and dispersion properties of PVC/$Mn_{0.5}Zn_{0.5}Fe_2O_4$ nanocomposite films. Optic. Mater. **118**, 111216 (2021)
24. M.I.A.A. Maksoud, S.M. Kassem, M. Bekhit, R.A. Fahim, A.H. Ashour, A.S. Awed, Gamma radiation shielding properties of poly(vinyl butyral)/Bi_2O_3@$BaZrO_3$ nanocomposites. Mater. Chem. Phys. **268**, 124728 (2021)
25. E. Şakar, Ö.F. Özpolat, B. Alım, M.I. Sayyed, M. Kurudirek, Phy-X / PSD: development of a user friendly online software for calculation of parameters relevant to radiation shielding and dosimetry. Radiat. Phys. Chem. **166**, 108496 (2020)
26. A. Acikgoz, G. Ceyhan, B. Aktas, S. Yalcin, G. Demircan, Luminescent, structural and mechanical properties of erbium oxide doped natural obsidian glasses. J. Non-Cryst. Solids **572**, 121104 (2021)
27. M. Fidan, A. Acikgoz, G. Demircan, D. Yilmaz, B. Aktas, Optical, structural, physical, and nuclear shielding properties, and albedo parameters of TeO_2–BaO–B_2O_3–PbO–V_2O_5 glasses. J. Phys. Chem. Solids **163**, 110543 (2022)
28. R. Divina, G. Sathiyapriya, K. Marimuthu, A. Askin, M.I. Sayyed, Structural, elastic, optical and γ-ray shielding behavior of Dy^{3+} ions doped heavy metal incorporated borate glasses. J. Non-Cryst. Solids **545**, 120269 (2020)
29. H.K. Obayes, H. Wagiran, R. Hussin, M. Saeed, Strontium ions concentration dependent modifications on structural and optical features of $Li_4Sr(BO_3)_3$ glass. J. Mol. Struct. **1111**, 132–141 (2016)
30. A. Al-Hajry, A. Soliman, M. El-Desoky, Electrical and thermal properties of semiconducting Fe_2O_3–Bi_2O_3–$Na_2B_4O_7$ glasses. Thermochim. Acta **427**(1–2), 181–186 (2005)
31. O.I. Sallam, A. Abdel-Galil, N.L. Moussa, Optimizing of optical and structure characters of borate glasses by different concentration of CoO: electron beam irradiation dosimetry. Mater. Chem. Phys. **269**, 124767 (2021)
32. O.I. Sallam, F.M. Ezz-Eldin, N.A. Elalaily, Influence of doping transition metals and irradiation on some physical properties of borate glass. Opt. Quant. Electron. **52**(4), 204 (2020)
33. A. Bajaj, A. Khanna, B. Chen, J.G. Longstaffe, U.W. Zwanziger, J.W. Zwanziger, Y. Gómez, F. González, Structural investigation of bismuth borate glasses and crystalline phases. J. Non-Cryst. Solids **355**(1), 45–53 (2009)
34. K.S. Shaaban, Y.B. Saddeek, K.A. Aly, A. Dahshan, Synthesis and physical characteristics of new glasses from some environmental wastes. SILICON **11**(5), 2445–2453 (2019)
35. A. Abdeldaym, O.I. Sallam, F.M. Ezz-Eldin, N.A. Elalaily, Influence of gamma irradiation on the optical, thermal and electrical features of blue commercial glass as potential accident dosimetry. J. Phys. Chem. Solids **157**, 110196 (2021)
36. H. Doweidar, Y.B. Saddeek, FTIR and ultrasonic investigations on modified bismuth borate glasses. J. Non-Cryst. Solids **355**(6), 348–354 (2009)
37. M. Salem, Structural characterization and gamma-ray shielding-parameters of some phosphate glasses containing By-Pass cement dust and barium oxide. Egypt. J. Chem. **64**(7), 2–3 (2021)
38. O. Sallam, A. Alhodaib, S. Abd El Aal, F. Ezz-Eldin, Influence of gamma ray on optical and structural properties of commercial glass enriched with copper oxide. Inorg. Chem. Commun. **124**, 108388 (2021)
39. C. Gautam, D. Kumar, O. Parkash, P. Singh, Synthesis, IR, crystallization and dielectric study of (Pb, Sr)TiO_3 borosilicate glass–ceramics. Bull. Mater. Sci. **36**(3), 461–469 (2013)
40. M.M. Ibrahim, M.A. Fanny, M. Hassaan, H. ElBatal, Optical, FTIR and DC conductivity of soda lime silicate glass containing cement dust and transition metal ions. SILICON **8**(3), 443–453 (2016)
41. M.V. Kumar, B. Jamalaiah, K.R. Gopal, R. Reddy, Optical absorption and fluorescence studies of Dy^{3+}-doped lead telluroborate glasses. J. Lumin. **132**(1), 86–90 (2012)
42. J. Dutchaneephet, A. Limpichaipanit, A. Ngamjarurojana, Optical spectroscopic investigations of neodymium and erbium added bismuth silicate glasses. Optik **178**, 111–116 (2019)
43. J. Dutchaneephet, A. Limpichaipanit, A. Ngamjarurojana, Spectroscopic property and color of bismuth silicate glasses with addition of 3d transition metals. Mater. Lett. **229**, 174–177 (2018)
44. M. El-Nahass, A. Ammar, A. Farag, A. Atta, E. El-Zaidia, Effect of heat treatment on morphological, structural and optical properties of CoMTPP thin films. Solid State Sci. **13**(3), 596–600 (2011)
45. B. Alshahrani, H.I. ElSaeedy, S. Fares, A.H. Korna, H.A. Yakout, M.I.A.A. Maksoud, R.A. Fahim, M. Gobara, A.H. Ashour, The effect of Ce^{3+} doping on structural, optical, ferromagnetic resonance, and magnetic properties of $ZnFe_2O_4$ nanoparticles. J. Mater. Sci. **32**(1), 780–797 (2021)

46. B. Alshahrani, H.I. ElSaeedy, S. Fares, A.H. Korna, H.A. Yakout, M.I.A.A. Maksoud, R.A. Fahim, A.H. Ashour, A.S. Awed, The effect of gamma irradiation on structural, optical, and dispersion properties of PVA/$Zn_{0.5}Co_{0.4}Ag_{0.2}Fe_2O_4$ nanocomposite films. J. Mater. Sci. **32**, 13336–13349 (2021)
47. A. El-Ghandour, A. Awed, M.A. Maksoud, M. Nasher, 1, 2-Dihydroxyanthraquinone: synthesis, and induced changes in the structural and optical properties of the nanostructured thin films due to γ-irradiation. Spectrochim. Acta Part A Mol. Biomol. Spectrosc. **206**, 466–473 (2019)
48. R. Chauhan, A.K. Srivastava, M. Mishra, K.K. Srivastava, Effect of UV exposure on some optical properties of As-Se based chalcogenide glasses. Integr. Ferroelectr. **119**(1), 22–32 (2010)
49. H. Zeyada, M. El-Nahass, I. Elashmawi, A. Habashi, Annealing temperatures induced optical constant variations of methyl violet 2B thin films manufactured by the spin coating technique. J. Non-Cryst. Solids **358**(3), 625–636 (2012)
50. A. El-Ghandour, M.F.O. Hameed, A. Awed, S. Obayya, Optical and electrical properties of nanostructured N,N′-diphenyl-N,N′-di-p-tolylbenzene-1,4-diamine organic thin films. Appl. Phys. A **124**(8), 543 (2018)
51. G.P. Singh, J. Singh, P. Kaur, S. Kaur, D. Arora, R. Kaur, D.P. Singh, Comparison of structural, physical and optical properties of Na_2O-B_2O_3 and Li_2O-B_2O_3 glasses to find an advantageous host for CeO_2 based optical and photonic applications. J. Non-Cryst. Solids **546**, 120268 (2020)
52. M.H.A. Mhareb, Y.S.M. Alajerami, M.I. Sayyed, N. Dwaikat, M. Alqahtani, F. Alshahri, N. Saleh, N. Alonizan, T. Ghrib, S.I. Al-Dhafar, Radiation shielding, structural, physical, and optical properties for a series of borosilicate glass. J. Non-Cryst. Solids **550**, 120360 (2020)
53. I. Akkurt, H. Akyıldırım, B. Mavi, S. Kilincarslan, C. Basyigit, Photon attenuation coefficients of concrete includes barite in different rate. Ann. Nucl. Energy **37**(7), 910–914 (2010)
54. P. Kaur, K.J. Singh, M. Kurudirek, S. Thakur, Study of environment friendly bismuth incorporated lithium borate glass system for structural, gamma-ray and fast neutron shielding properties. Spectrochim. Acta Part A **223**, 117309 (2019)
55. E. Yılmaz, H. Baltas, E. Kırıs, İ Ustabas, U. Cevik, A. El-Khayatt, Gamma ray and neutron shielding properties of some concrete materials. Ann. Nucl. Energy **38**(10), 2204–2212 (2011)
56. V.P. Singh, N. Badiger, J. Kaewkhao, Radiation shielding competence of silicate and borate heavy metal oxide glasses: comparative study. J. Non-Cryst. Solids **404**, 167–173 (2014)
57. M.M. Rafiei, H. Tavakoli-Anbaran, Calculation of the exposure buildup factors for x-ray photons with continuous energy spectrum using Monte Carlo code. J. Radiol. Prot. **38**(1), 207–217 (2018)
58. P. Basu, R. Sarangapani, B. Venkatraman, Gamma ray buildup factors for conventional shielding materials and buildup factors computed for tungsten with a thickness beyond 40 mean free paths. Appl. Radiat. Isot. **154**, 108864 (2019)

Publisher's Note Springer Nature remains neutral with regard to jurisdictional claims in published maps and institutional affiliations.